Performance and Facility Background Pressure Characterization Tests of NASA's 12.5-kW Hall Effect Rocket with Magnetic Shielding Thruster

IEPC-2015-07 /ISTS-2015-b-07

Presented at Joint Conference of 30th International Symposium on Space Technology and Science
34th International Electric Propulsion Conference and 6th Nano-satellite Symposium,
Hyogo-Kobe, Japan
July 4 – 10, 2015

Hani Kamhawi,[1] Wensheng Huang,[2] Thomas Haag,[3] Rohit Shastry,[4] Robert Thomas,[5] John Yim,[6] Daniel Herman,[7]
NASA Glenn Research Center, Cleveland, Ohio, USA

George Williams[8]
Ohio Aerospace Institute, Cleveland, Ohio, USA

James Myers[9]
Vantage Partners LLC, Cleveland, Ohio, USA

and

Richard Hofer,[10] Ioannis Mikellides,[11] Michael Sekerak,[12] and James Polk[13]
Jet Propulsion Laboratory, California Institute of Technology, Pasadena, California, USA

NASA's Space Technology Mission Directorate (STMD) Solar Electric Propulsion Technology Demonstration Mission (SEP/TDM) project is funding the development of a 12.5-kW Hall thruster system to support future NASA missions. The thruster designated Hall Effect Rocket with Magnetic Shielding (HERMeS) is a 12.5-kW Hall thruster with magnetic shielding incorporating a centrally mounted cathode. HERMeS was designed and modeled by a NASA GRC and JPL team and was fabricated and tested in vacuum facility 5 (VF5) at NASA GRC. Tests at NASA GRC were performed with the Technology Development Unit 1 (TDU1) thruster. TDU1's magnetic shielding topology was confirmed by measurement of anode potential and low electron temperature along the discharge chamber walls. Thermal characterization tests indicated that during full power thruster operation at peak magnetic field strength, the various thruster component temperatures were below prescribed maximum allowable limits. Performance characterization tests demonstrated the thruster's wide throttling range and found that the thruster can

[1] Ion Propulsion System (IPS) Thruster Deputy Lead and Senior Research Engineer, Electric Propulsion Systems Branch, hani.kamhawi-1@nasa.gov
[2] IPS Thruster Diagnostics Lead and Research Engineer, Electric Propulsion Systems Branch
[3] IPS Mechanical Engineer and Senior Research Engineer, Electric Propulsion Systems Branch
[4] IPS Thruster Diagnostics Engineer and Research Engineer, Electric Propulsion Systems Branch
[5] IPS Thruster Engineer and Research Engineer, Electric Propulsion Systems Branch
[6] IPS Modeling and Simulation Engineer, Research Engineer, Electric Propulsion Systems Branch
[7] IPS Lead and Senior Engineer, Electric Propulsion Systems Branch
[8] IPS Thruster Wear Testing Lead, Senior Research Engineer
[9] IPS Thruster Thermal Engineer and Senior Aerospace Engineer
[10] IPS Thruster Lead and Senior Engineer
[11] IPS Modeling and Simulation Lead and Principal Engineer
[12] IPS Thruster Engineer
[13] IPS Deputy Lead and Principal Engineer

achieve a peak thruster efficiency of 63% at 12.5 kW 500 V and can attain a specific impulse of 3,000 s at 12.5 kW and a discharge voltage of 800 V. Facility background pressure variation tests revealed that the performance, operational characteristics, and magnetic shielding effectiveness of the TDU1 design were mostly insensitive to increases in background pressure.

Nomenclature

A_i	=	exit area
ARM	=	Asteroid Redirect Mission
BaO	=	barium oxide
EP	=	electric propulsion
HEOMD	=	Human Exploration and Operations Mission Directorate
HERMeS	=	Hall effect rocket with magnetic shielding
HS	=	high speed
IG	=	ion gauge
IR	=	infrared
k_b	=	Boltzmann constant
LaB_6	=	lanthanum hexaboride
MFC	=	mass flow controller
MSCT	=	magnetic shielding characterization test
m_{xe}	=	xenon molecular mass
N_B	=	boron nitride normalized signal strength
OES	=	optical emission spectroscopy
P	=	pressure
P2P	=	peak to peak
$P2P/I_d$	=	peak to peak to discharge current ratio
QCM	=	quartz crystal microbalance
SEP	=	solar electric propulsion
STMD	=	Space Technology Mission Directorate
TDM	=	Technology Demonstration Mission
TDU	=	technology development unit
T_n	=	neutral temperature
VF5	=	vacuum facility 5
WFS	=	Wien filter spectrometer

I. Introduction

High-power electric propulsion (EP) systems are enabling and enhancing for time-critical missions or missions requiring transportation of large payloads. A number of mission studies were performed over the last decade which highlight the enhancing and enabling features of high-power EP systems for reusable space tug applications for transfer of payloads from low-Earth-orbit (LEO) to geosynchronous-Earth-orbit (GEO) and for use in Mars mission scenarios.[1,2,3,4,5,6,7]

NASA's Space Technology Mission Directorate (STMD) is sponsoring the development, maturation, and evaluation of the key technologies needed to reduce the cost and expand the capability of future space exploration activities. One of the projects under STMD is the Solar Electric Propulsion (SEP) project. The SEP project's major activities are the development of large deployable solar array structures and the high-power EP system (Hall thruster and power processing unit) that can meet NASA's near term science and exploration needs but are also extensible to NASA's future human exploration needs. The NASA Glenn Research Center (GRC) is partnering with the Jet Propulsion Laboratory (JPL) to carry out the Hall thruster development work. The SEP Technology Demonstration Mission (TDM), initially announced in 2011, is aimed at demonstrating new cutting edge technology in flexible solar arrays and electric propulsion that will increase the maturity of these key SEP technologies for future commercial and government uses. Once these technologies have been demonstrated, they are expected to enable higher performance LEO-to-GEO transfers as well as a number of other near-Earth orbit transfers and station-keeping maneuvers. These technologies may also benefit a potential robotic mission to redirect an asteroid into cis-lunar orbit for crew

exploration. In longer terms, these technologies will reduce mission costs for NASA interplanetary robotic missions in general, and will serve as a precursor to higher power systems for human interplanetary exploration. Human and robotic exploration beyond LEO will require enabling capabilities that are efficient, affordable, and reliable. SEP is highly advantageous because of its favorable in-space mass transfer efficiency compared to traditional chemical propulsion systems. SEP stages have the potential to be the most cost effective solution to perform beyond LEO transfers of high mass payloads for human missions. Recognizing that these missions require power levels more than 10 times greater than current electric propulsion systems, NASA embarked upon a progressive pathway to identify critical technologies needed and a plan for a SEP TDM. The four top-level objectives of the SEP TDM Project, detailed in References 4, 5, and 8 are as follows:

- perform an in-space demonstration that advances the maturity of high-power EP technology and high-power solar array power system technology in relevant space environments and operational regimes;
- demonstrate integrated SEP spacecraft design, fabrication, and test as well as operational modes associated with orbit transfer;
- demonstrate extensible high-power EP and solar array power system technologies and integrated SEP spacecraft operational modes that can be adapted for use in next-generation, higher power SEP systems; and
- provide a SEP-based transportation capability with performance advancements over those previously demonstrated.

One of the NASA in-house concepts is the Asteroid Redirect Mission (ARM) involving a partnership with the STMD and Human Exploration and Operations Mission Directorate (HEOMD). The ARM concept uses a robotic spacecraft equipped with a high power, SEP system to rendezvous with, capture, and redirect a small asteroid with a mass of up to 1,000 tons to a long-term, stable lunar orbit.[9] Because ARM is enabled by high-power solar array and EP technologies, it is an ideal platform to meet the needs of STMD's SEP TDM. ARM would demonstrate deployment and operation of a new class of large, lightweight, high-specific-power, flexible-blanket solar arrays in space along with the operation of a high-power, high-performance EP system. As such, STMD is also making investments in critical power technologies required for high-power SEP. The Solar Array System contracts are developing two different 15 to 25 kW solar array wing technologies that are extensible to higher power. Figure 1 shows an artist rendition of the ARM spacecraft.

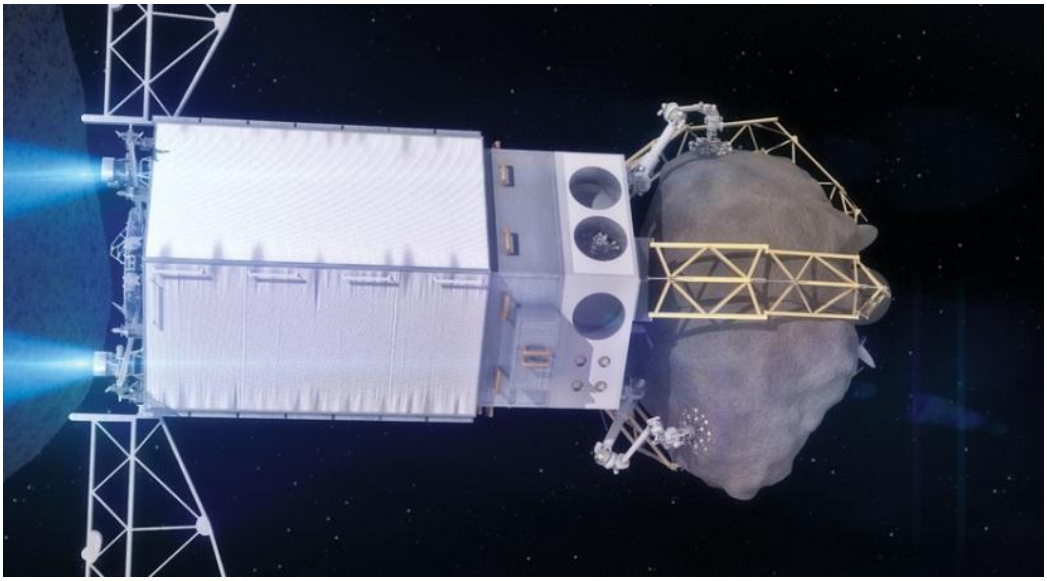

Figure 1. Conceptual artist rendition of the ARM spacecraft. NASA is developing ARM, the first robotic mission to visit a large near-Earth asteroid, collect a multi-ton boulder from its surface, and redirect it into a stable orbit around the moon.

The proposed SEP TDM missions are baselining EP systems that utilize 12.5 kW-class, long-life Hall thruster strings.[10] The NASA GRC and JPL team development of a long-life capable, 12.5 kW, magnetically-shielded Hall thruster was enabled by two major events: (1) Aerojet Rocketdyne designed and built the BPT-4000 that demonstrated a zero-erosion state after 5,600 h of qualification testing,[11] and (2) the JPL performed numerical simulations that explained the physics behind these test results.[12,13,14] Knowledge gained from applying magnetic-shielding circuit

design approach in these two Hall thrusters is leveraged in the design and construction of the 12.5 kW Hall thruster designated Hall Effect Rocket with Magnetic Shielding (HERMeS).

This paper present the performance and facility background pressure test results for the HERMeS technology development unit 1 (TDU1). In addition, this paper summarizes key findings form the thermal characterization, magnetic shielding characterization, and optical probe measurements. The paper is organized as follows: section 2 provides a brief summary of the TDU1 thruster design and fabrication; section 3 presents the experimental apparatus; section 4 presents a brief summary of the findings from the TDU1 thruster various tests including: plasma plume mappings , thermal characterization , magnetic shielding characterization , and optical probe characterization tests; section 5 presents the results from the thruster performance characterization test; section 6 presents the results from the thruster facility background pressure characterization test; and section 7 provides a summary of the paper.

II. HERMeS TDU1 and TDU2 Thrusters Design and Fabrication

The 12.5 kW HERMeS thruster magnetic circuit and scaling design activity leveraged JPL's H6MS and NASA GRC's 300MS extensive thrusters design and test experiences.[14,15,16] The thruster scaling was based on heritage NASA Hall thruster designs. Three candidate thruster heritage configurations were evaluated. Key downselect criteria included the throughput capability and performance characteristics of all three configurations. Other selection criteria considered included: magnetic circuit saturation margin, inner magnetic circuit volume and thermal margin, and thruster configuration heritage. Extensive plasma, magnetic, flow, thermal, and structural modeling was performed in support of the thruster design activity. A companion paper by Hofer presents a detailed overview of the thruster design activities.[17]

NASA GRC is fabricating two TDU thrusters. TDU1 was extensively tested at NASA GRC and TDU2 will be initially tested at NASA GRC but will then be shipped to JPL for environmental tests. The TDU1 thruster fabrication, assembly and functional testing were performed at NASA GRC. A photograph of this thruster is shown in Fig. 2. Initial functional testing included a detailed propellant manifold flow mapping[18] and a detailed magnetic field mapping. Then, a hot firing tests were performed to evaluate the thruster performance and assess the thruster stability, magnetic shielding, and thermal stability.

The HERMeS thruster baseline configuration and mechanical design was guided by the thruster scaling and the subsequent magnetic and plasma simulations. Thruster scaling provided the dimensions for the discharge chamber. The HERMeS thruster magnetic circuit model provided the dimensions of the various thruster magnetic circuit components. The thruster mechanical design leveraged NASA GRC's and JPL's experience and lessons learned with the design of the NASA-457Mv1&v2, NASA-300M, NASA-120, NASA-173, H6MS, and HiVHAc. Some of the unique HERMeS thruster design features include:

- a monolithic boron nitride (BN) discharge chamber;
- a magnetically-shielded field topology;
- a reverse flow propellant manifold with enhanced flow uniformity and protection from backsputtered materials deposition;
- a radiator attached to the thruster's backpole for enhanced heat rejection;
- a design capable of withstanding the projected structural and thermal loads for a range of NASA TDMs; and
- a centrally mounted cathode.

Two hollow cathode assemblies, shown in Fig.3, were designed for the TDU thruster and they are:

- Assembly 1: Uses a barium oxide (BaO) impregnated porous tungsten thermionic emitter. This assembly design is based on the discharge cathode design for NASA's Evolutionary Xenon Thruster (NEXT) that has recently completed over 50,000 hrs of operation.[19]
- Assembly 2: Uses a lanthanum hexaboride (LaB6) emitter that has been used on the flight SPT-100 and PPS-1350 thrusters and used in the H6MS thruster. Use of LaB6 emitter eases handling assembly requirements and reduces the propellant purity requirements.[20] However, the LaB6 emitter operates at higher peak temperatures than the BaO impregnated emitter and will require the qualification of new U.S. made heaters.

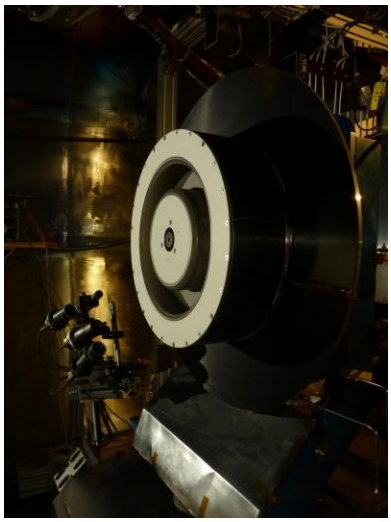

Figure 2. Photograph of the 12.5-kW TDU1 thruster inside VF5.

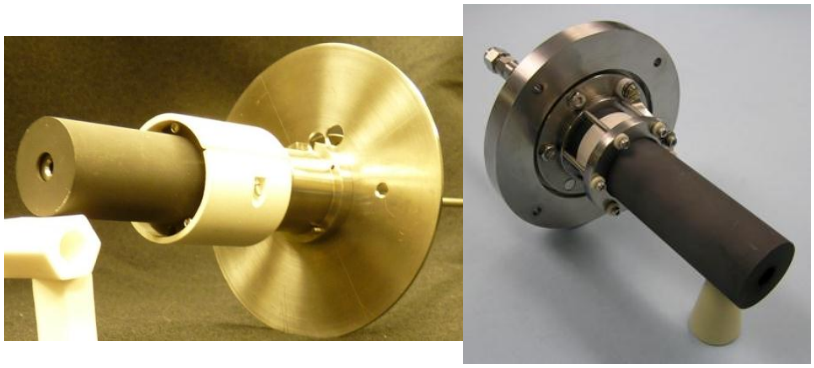

Figure 3. Photographs of hollow cathode assembly 1 (left) and assembly 2 (right).

Detailed description of the thruster design approach is provided in a companion paper[17] and previously in Reference 21.

Finally, TDU2 thruster fabrication is ongoing and is expected to be completed in September of 2015. Minor design changes and new features are being incorporated in TDU2 to maintain the thruster's discharge channel precise alignment during thruster operation. These changes were performed to assure that the thruster can withstand and pass the environmental test sequence.

III. Experimental Apparatus

This section details the experimental apparatus that was employed during the TDU1 thruster test campaign at NASA GRC. This section will provide an overview of the vacuum facility, the xenon propellant feed system, laboratory power console, inverted pendulum thrust stand, data acquisition system, and diagnostics employed during the test.

A. Vacuum Facility 5

Testing of the TDU1 thruster was performed in vacuum facility 5 (VF5) at NASA GRC. The main chamber of is 4.6 m in diameter and 18.3 m long. VF5 can be evacuated with cryopanels and oil diffusion pumps. For this test campaign, the TDU1 thruster was placed in main volume of the chamber to assure that the lowest possible background pressure conditions were attained during thruster operation. Figure 4 shows a picture of the TDU1 thruster mounted inside VF5. Facility pressure was monitored with four ion gauges accurate to ±2% of reading according to manufacturer's specifications. Modeling of the flow inside VF5 was used to inform the location and orientation of the ion gauges.[22] Three gauges, designated 1 to 3 displayed xenon corrected pressure readings and were mounted next to the thrust stand, approximately 0.8 m from the thruster and aligned with exit plane. Ion gauge 1 is facing downstream while ion gauges 2 and 3 are orthogonal to downstream propellant flow direction. Ion gauge 1 reports 1.5 times the reading of ion gauge 2, while ion gauges 2 and 3 agree to within 10% of each other. Ion gauge 2 readings were used to determine the number of multiples of the lowest achievable background pressure that the thruster was experiencing. The fourth gauge was on the facility chamber wall mid section. All reported ion gauge readings are corrected for xenon. The locations of the gauges are shown in Fig. 4 (right).

B. Laboratory Propellant Feed System

A laboratory propellant feed system was used in the TDU1 test campaign. The feed system supplied xenon to the thruster and was also used to elevate the background pressure in VF5. The propellant feed system utilized four mass flow controllers (MFCs). A 500 and a 100 sccm MFCs supplied xenon propellant to the thruster and cathode,

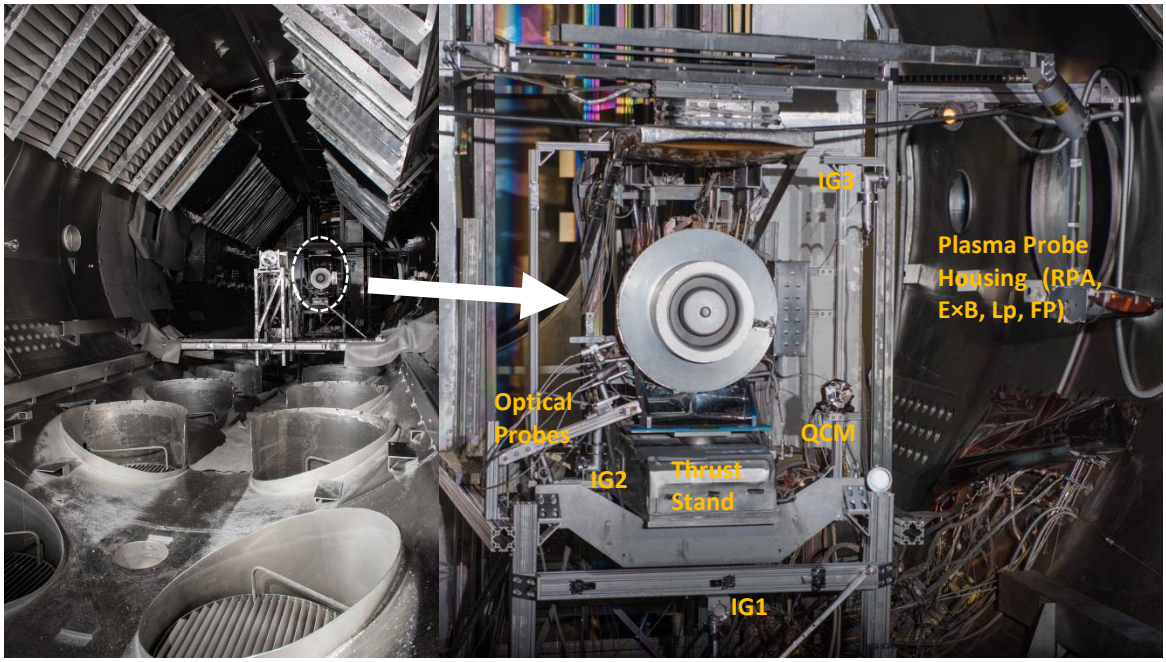

Figure 4. Photograph of TDU1 thruster installed in VF5 main volume (left). Close up photograph of TDU1 thruster showing the location of the ion gauges, QCM, and Plasma probe rake (right).

respectively. A 1,000 sccm flow controller supplied xenon to elevate the chamber pressure. The 200 sccm MFC was not used during this test campaign. The MFCs calibration curves indicated that the anode and cathode flow rates uncertainty is ≤1% of set value.

C. Power Console

For this test campaign the thruster was powered with a laboratory power rack that contained the discharge, inner and outer electromagnet, cathode heater, and cathode keeper power supplies. The discharge power supply consists of three 15 kW (1000 V and 15 A) power supplies that were connected in a master-slave configuration. A computer was used to sweep the thruster discharge voltage during the thruster stability characterization test.

D. Inverted Pendulum Thrust Stand

A null-type, water-cooled, inverted-pendulum thrust stand was used during thruster performance evaluation. The power cables were fed from the vacuum feedthroughs to the thruster using a "waterfall" configuration to minimize the thermal drift of the thrust stand readings. In-situ thrust stand calibrations were performed prior to, during, and after thruster testing. In addition, the thruster was periodically turned off during testing to measure the thrust stand thermal drift magnitude. Corrections were incorporated in the reported thrust. Thrust measurement uncertainty was estimated at 2% of measured value.

E. Data Acquisition

A data logger was used to measure and record the thruster operating parameters. End-to-end calibrations were performed using a calibrated meter and they included the various thruster operating currents, operating voltages, thruster component temperatures, and research ion gauge pressure measurements in the vicinity of the thruster.

F. Diagnostics

An extensive set of diagnostics was used to take full advantage of the opportunity to test the TDU1 in VF5. Figure 5 shows a layout of the various diagnostics that were employed during the TDU1 thruster test campaign in VF5. These diagnostics included:

- plasma diagnostics that were mounted on an axial stage and rotary stage. These included Faraday, retarding potential analyzer (RPA), E×B, and Langmuir probes. The plasma diagnostics test results will be reported by Huang at an upcoming conference;
- sixteen flush-mounted Langmuir probes that were placed along the discharge channel walls to measure the local plasma potential and electron temperature. Detailed test results will be reported by Shastry at the AIAA Propulsion and Energy Forum 2015;[23]
- high-speed video imaging of the TDU1 thruster discharge was performed using a high speed camera. Analysis of the high speed videos will be reported by Huang in an upcoming conference;
- type-K thermocouples were used to monitor the temperature of various thruster components during this test campaign. Analysis of the results is on-going and will be reported by Myers at an upcoming conference;
- infrared camera was placed inside a pressurized enclosure inside VF5 approximately 5 m away from the thruster. Results from the thermocouple and IR camera measurements will also be presented by Huang at an upcoming conference. Results from the IR camera will be reported by Huang et al. at the AIAA Propulsion and Energy Forum 2015;[24] and
- optical probes were constructed using 1.25 cm diameter UV-silica lenses, flat windows, optical tubes, and SMA fiber optic connections. Results of the optical measurement were reported by Williams et al. in Reference 25.

IV. TDU1 Thruster Test Campaign Overview

The TDU1 thruster was subjected to an extensive set of tests at NASA This section provides a summary of the TDU1 thruster tests: plasma diagnostics plume characterization test, thermal characterization test, magnetic shielding characterization test, and optical characterization test. These set of tests were performed before performing the thruster's performance and facility background pressure characterization tests.

A. Plasma Diagnostics Plume Characterization

A variety of plasma diagnostics were simultaneously deployed to the various objectives of the test. These diagnostics include far-field Faraday probe, retarding potential analyzer (RPA), accompanying Langmuir probe, Wien filter spectrometer (WFS), high-speed (HS) camera system, and infrared (IR) camera system. Figure 5 shows a diagram of the diagnostics setup in the vacuum facility.

The far-field Faraday probe, RPA, accompany Langmuir probe, and WFS form the probe array. The probe array is mounted on a two-axis polar positioning system. Data collected include current density, ion energy per charge, and species composition as functions of angle and distance. These data will be used for spacecraft interaction, thruster performance, and facility effect studies. Results of the spacecraft interaction studies will provide guidelines for the design of vehicles that may use HERMeS, including the Asteroid Redirect Vehicle. The thruster performance studies will be used to characterize and form a baseline for various aspects of the thruster that can affect its performance and life. The results of both studies will also be projected to a space-like environment in order to predict on-orbit thruster and plume characteristics as well as differences from ground-test characteristics.

The HS camera system comprise of the camera, located outside the vacuum facility, and a mirror, located inside. The mirror is positioned such that it is slightly below the firing axis of the thruster so that it does not obstruct the view of the IR camera. The center of the mirror is located about 5 degrees from the firing axis of the thruster. The effective distance from the HS camera to the thruster is approximately 6.5 m. Data from the HS camera will be used to help determine the magnetic field margin, the plasma oscillation characteristics, and be used in the facility-effect study. The plasma oscillations characteristics will help define the range of magnetic field over which the thruster would operate on-orbit while avoiding excessive oscillations and aid in the design of appropriate filters for the power processing unit.

The IR camera system comprise of the IR camera, located approximately 6 m downstream of the thruster on the firing axis, and the IR camera calibration array, located in the immediate vicinity of the thruster slightly upstream of the thruster radiator. The primary function of the IR camera system is to provide data that are complimentary to the thruster-embedded thermocouples. The combined set of thermal data will be used to refine and validate the thruster thermal model. The secondary function of the IR camera system is to identify any localized or transient thermal

anomalies that may be present support thermal design optimization. Detailed analysis of the IR camera measurement will be presented by Huang at the AIAA Propulsion and Energy Forum.[24] Figure 6 shows a representative Faraday probe ion beam profile at 12.5 kW and 800 V thruster operation (left) and the corresponding RPA probe trace at the same operating condition (right).

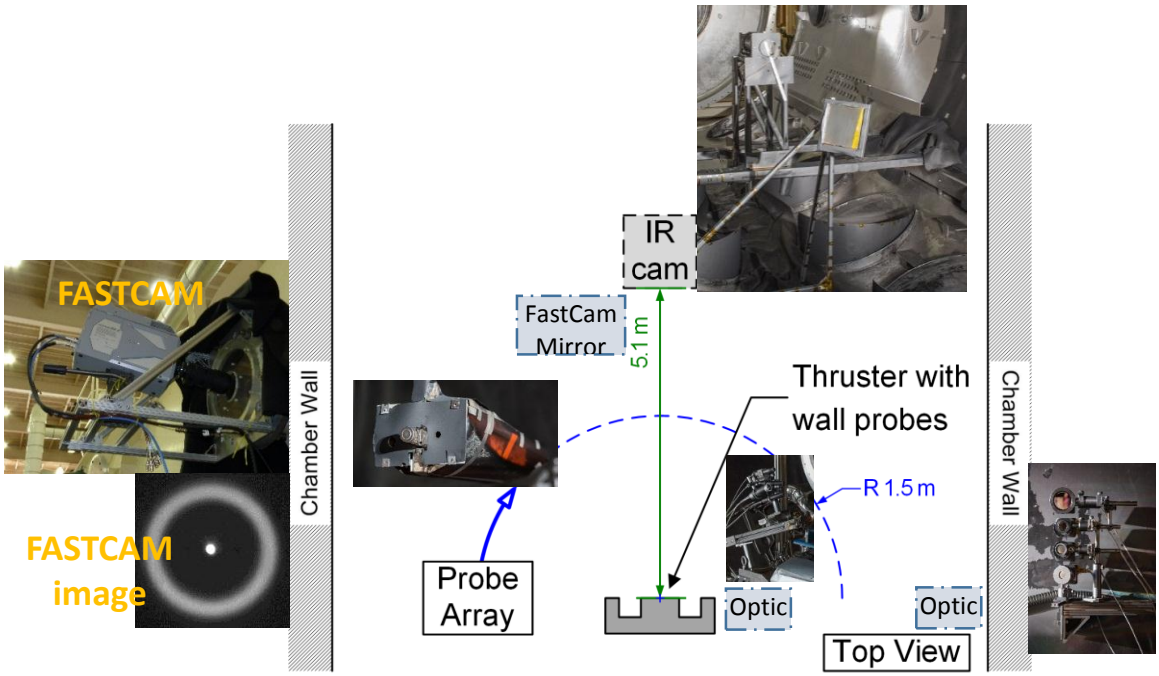

Figure 5. Diagram showing layout of diagnostics employed during the TDU1 thruster at NASA GRC's VF5.

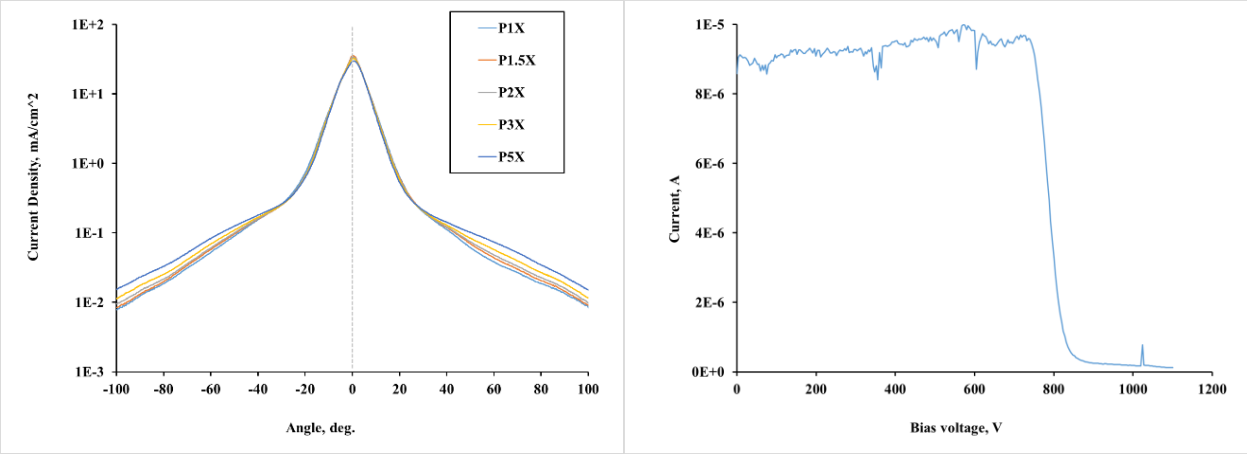

Figure 6. Faraday probe ion beam plume profiles (left) and RPA trace along thruster center line (right) during TDU1 thruster operation at 12.5 kW 800 V.

B. Thermal Characterization Test Summary and Thermal Model Development

Thermal characterization tests of the TDU1 thruster were performed to confirm that the steady state operating peak temperatures of the thruster's various components are below the engineering limit temperatures and to provide data for validation of the thruster's thermal model. The tests of the TDU1 thruster were performed at 9.4 kW and a discharge voltage of 300V and 12.5 kW at discharge voltages of 400, 500, 600, 700, and 800 V. At 12.5 kW and 800 V thruster operation, steady-state thermal characterization tests were performed at the nominal thruster magnetic field setting and at the maximum thruster magnetic field setting. Column 2 of Table 1 presents a summary of the critical components temperatures. Results of the tests are still being analyzed but indicated that the highest thruster temperatures were attained during 12.5 kW and 800 V thruster operation and that the measured temperatures are within the prescribed maximum allowable temperatures. Detailed presentation of the thruster thermal characterization test results will be presented at an upcoming conference.

An analytical thermal model of the HERMeS Hall thruster was developed during the design phase to aid decisions about hardware features to improve the thruster's heat rejection capability. The model represents the physical hardware of the thruster, excluding the cathode, power and control electronic subsystems. Its primary purpose is to predict component temperatures to ensure they remain within their maximum allowable temperature limits at all operating conditions. The model includes a medium fidelity representation of the VF5 vacuum tank facility (including cryo-panels) to accurately model the thruster's thermal environment. The model currently predicts steady-state thruster temperatures, with only the electromagnets operating, to within 1 ˚C of the test data.

Table 1. TDU1 steady state thermal characterization test and model temperature results comparison for selected thruster components for thruster operation at 12.5 kW 800 V and at peak magnetic field strength

	Test , ºC	Model, ºC
Outer Discharge Channel	**545**	**530**
Inner Discharge Channel	**539**	**530**
Discharge Channel Base	**501**	**485**
Outer Electromagnet	**391**	**370**
Inner Electromagnet	**452**	**508**
Thruster Inner Bore	**436**	**433**
Inner diameter of Backpole	**414**	**415**
Radiator ID	**371**	**368**
Radiator OD	**306**	**301**

The model simulates the thermal performance of the thruster. Heat loads due to plasma interactions with discharge channel walls were predicted by a JPL developed code, Hall2De [26]. Heat load predictions from Hall2De were applied as boundary conditions on the discharge channel and inner front pole. The thermal model accounts for all conductive and radiative exchange of thermal energy. Currently, all solutions are steady-state representing worst-case peak temperatures of the thermal design. The thruster model contains 9,608 thermal nodes over 19 component submodels. Test data comprised of component temperatures and magnet coil currents have been used for model correlation. Operational data has shown thruster temperatures are a function of discharge power and voltage and B-field intensity. The model was tuned to match the temperatures for the maximum operating condition of 12.5 kW and 800V, and peak magnetic field operating conditions from the most recent thermal characterization tests. The resultant model-to-test temperature comparison is shown in Table 1 and indicates excellent agreement between the model and test results (within 20 ºC) except for the inner coil temperature where the model over predicts the temperature. The model is continually being refine but it is being used to thermally assess vehicle integration strategies, requirements, and in-space mission scenarios.

C. Magnetic Shielding Characterization Test (MSCT)

The MSCT was performed on the TDU1 thruster in order to determine the degree of magnetic shielding in the thruster at the operating conditions shown in Table 2. Eight flush-mounted Langmuir probes were placed along each channel wall to measure the local plasma potential and electron temperature. Figure 7 shows a diagram of the axial locations of each probe with respect to the thruster exit plane. Axial locations were identical between the inner and outer channel walls. While the majority of the probes were concentrated in the chamfer region of the channel to characterize the magnetic shielding, additional probes were placed further upstream in order to determine relative plasma number densities that would elucidate the plasma power deposition profile on the walls.

Table 2. Summary of operating conditions where probe data were collected. Additional data were collected at 300 V and 9.4 kW at various magnetic field strengths and facility backpressures.

Discharge Voltage [V]	Discharge Power [kW]
300	4.7
300	9.4
400	12.5
500	12.5
600	12.5
700	12.5
800	12.5

Table 3. Summary of results from critical probes at select operating conditions. Plasma properties at the channel walls indicate an excellent degree of magnetic shielding even at elevated discharge voltages.

	300 V, 9.4 kW				800 V, 12.5 kW			
	Probe #5		*Probe #2*		*Probe #5*		*Probe #2*	
	Inner Wall	Outer Wall	Inner Wall	Outer Wall	Inner Wall	Outer Wall	Inner Wall	Outer Wall
Plasma Potential [V]	307	307	306	308	N/A	808	809	809
Electron Temperature [eV]	3	3	3	5	N/A	3	3	4

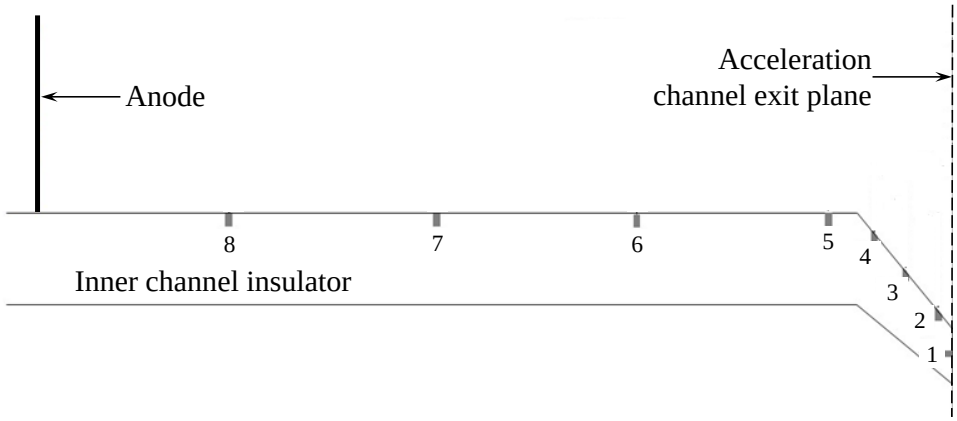

Figure 7. Location of the wall probes installed along the inner channel wall of TDU1 thruster for the purpose of verifying magnetic shielding has been achieved. The locations of the probes along the outer wall were identical to those shown here along the inner wall.

These data would aid thermal and plasma modeling efforts at GRC and JPL. However, probes #2 and #5 were deemed critical towards the confirmation of magnetic shielding in HERMeS. This is because probe #2 is expected to have the lowest plasma potential and highest electron temperature within the channel, while the properties at probe #5 are highly sensitive to the location of the grazing magnetic field line across the chamfer.

Parametric studies were also performed at 300 V, 9.4 kW to determine the sensitivity of the magnetic shielding to magnetic field strength and facility backpressure. All these data will be presented in detail by Shastry at the AIAA Propulsion and Energy Forum 2015.[23]

Table 3 shows the probe results from the critical probes (#2 and #5) along the inner and outer channel walls for the 300 V at 9.4 kW and 800 V at 12.5 kW operating conditions at nominal facility pressure and optimized magnetic

field strength. All plasma potentials were measured with respect to cathode common. Data could not be collected with probe #5 on the inner wall due to probe insulation breakdown at the high discharge voltage. It is evident that the degree of magnetic shielding is excellent even at the high discharge voltage of 800 V. The data show that the predicted ion beam energies at the wall will be negligible up to the thruster exit plane, and the predicted sheath energies will be ≤ 40 eV. With such low ion impingement energies at the walls, channel erosion is not expected to be a life-limiting mechanism in the HERMeS thruster.

D. Optical Diagnostics

The use of fiber optic probes to characterize the wear and operation of HERMeS thrusters has been demonstrated.[25] Optical probes were constructed using 1.25 cm diameter UV-silica lenses and flat windows, optical tubes, and SMA fiber optic connections. Lenses which matched the acceptance angle of the 400 μm diameter UV-VIS fiber optic cables and protective windows were incorporated in all of the probes. For those probes focused on the BN surface, a second lens with a 30 cm or 50 cm focal length was incorporated in a threaded section which allowed adjustment of the focal point. Single-fiber, metal-jacketed, fiber-optic cables and vacuum feedthroughs connected the probes to a fiber-optic multiplexer located external to the vacuum chamber.

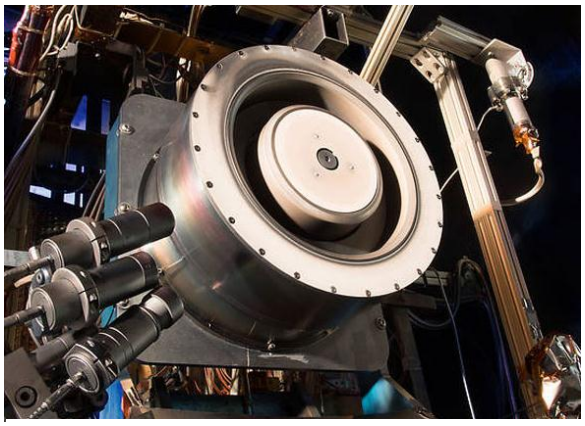

Figure 8. Photograph of the HERMeS thruster used in this investigation. Optical probes are shown to the lower left.

Five optical probes were mounted near the thruster outside of a 45° exclusion zone on a 50 mm travel linear translation stage. Four of those probes were used to interrogate the plume of the thruster. These were collimated to cylindrical volumes of 2 mm in diameter. As the stage translated downstream of the exit plane, the point of interrogation of the fifth probe moved across the face of the thruster. However, its primary region of interrogation was the chamfered lip of the inner boron nitride insulator. Figure 8 shows a photograph of the probes to the lower left of the TDU1 thruster in VF5.

The probes were calibrated before, during, and after each test. Standard xenon and tungsten lamps were placed at the same distance as the location of measurement in the thruster for each probe. Spectral data were recorded using the entirety of the probe-fiber-feed thru system before and after each series of testing. This measured the transmission function of the different probe assemblies which was used in the reduction of the data. Minor variations were noted which were likely the result of sputter deposition on the protective windows. The deposition tended to preferentially reduce the signal strength below a wavelength of 350 nm. However, the degradation was negligible. Calibrations were performed during a test sequence by recording spectra at repeated thruster operating conditions. No significant changes in line intensities were noted, and the slight degradation of the UV signal was recorded and used in the normalization of the data.

Trends in the singly-ionized xenon spectra were converted to a basic approximation of Xe II number density. Use of an onion-peeling technique yielded rough spatial resolution of the near-field plume. In particular, the technique captured changes in the plasma structure associated with changes in the peak magnetic field strength and discharge voltage. Correlation of the Xe II OES data with far field plume measurements remains to be completed. Preliminary calculations of electron temperature yielded values that are consistent with expectations for ionization and near-field plume regions. Complete correlation should yield a very comprehensive characterization of the near-field plasma without intrusion of physical probes. Insulator erosion trends characterized by the normalized boron neutral atom spectral emission at 250 nm were obtained. The N_B (normalized signal strength for the boron transition) values were negligible across the inner channel for all nominal operating conditions as is shown in Fig. 9. They were observed to slightly decrease at higher than nominal magnetic field settings. This further confirms that the thruster is magnetically shielded for all operating conditions across its throttling range. Carbon OES near the cathode keeper shows that the erosion of the cathode keeper is more of a concern at high discharge voltages. Details of the optical measurements study are presented in Reference 25.

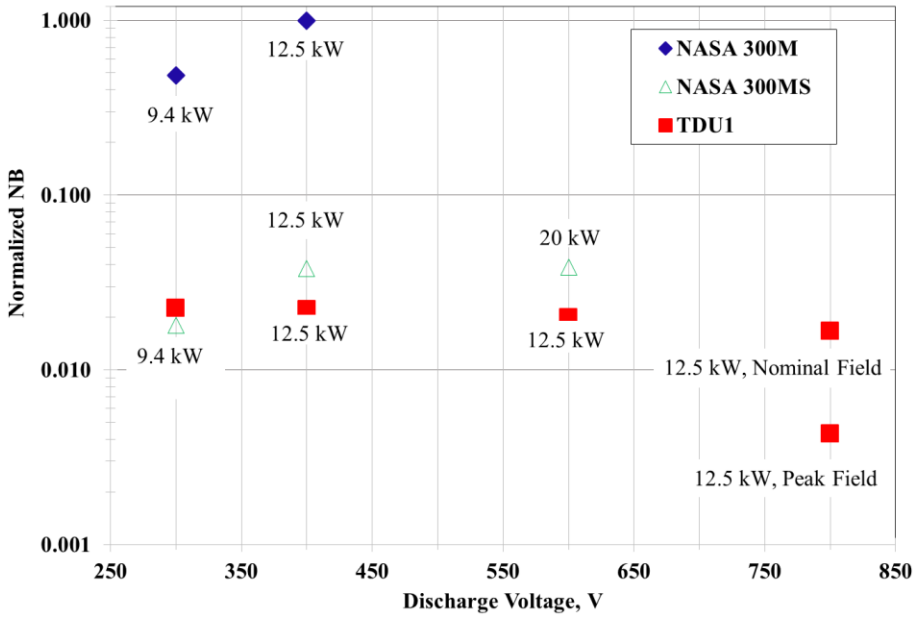

Figure 9. Comparison of boron nitride signal strengths indicating magnetic shielding at all operating conditions. Two data points from NASA 300M and NASA 300MS operation at similar powers are given.[25]

V. TDU1 Thruster Performance Characterization Test Results and Discussion

Performance of the TDU1 thruster was characterized at various thruster operating conditions over a discharge voltage range of 300 and 800 V and discharge power levels between 0.6 and 12.5 kW. Table 4 lists the thruster operating conditions where the thruster performance was evaluated. Unsuccessful attempts were made to operate the thruster at power levels below 6.25 kW for 700 V and 9.4 kW for 800 V. During these tests, which were characterized by P2P/Id % magnitudes of over 200%, steady state thruster operation was not achieved and the discharge current continued to rise. This is similar to trends observed during tests of the H6MS.[14]

Table 4. TDU1 thruster operating conditions during the thruster's performance characterization test

	Discharge Power, kW								
Discharge Voltage	**0.6**	**1.5**	**2**	**2.5**	**3**	**4.7**	**6.25**	**9.4**	**12.5**
300	√	√	√		√	√	√	√	√
400			√			√	√	√	√
500				√			√	√	√
600					√		√	√	√
700							√	√	√
800								√	√

The thruster performance characterization was preceded by the thruster bakeout, thermal characterization test, and MSCT. During the TDU1 thruster performance evaluation the cathode flow rate was set at approximately 7% of the anode flow rate. The optimal magnetic field setting of the thruster was found by minimizing the discharge current for a given thruster flow rate while attaining a reasonable discharge current peak-to-peak to discharge current ($P2P/I_d$) oscillation levels. Once the optimal magnetic field setting was found, the thruster discharge was allowed to stabilize for at least 10 minute before thruster performance data was recorded. The thrust stand thermal drift was quantified prior to performance characterization test and periodic thruster shutdowns. During full power thruster operation at 400 V, the total TDU1 xenon flow rate was ~30 mg/s with a corresponding ion gauge 2 pressure reading of 6.6 μTorr-Xe, whereas, during 800 V full power operation the TDU1 total flow rate was ~18 mg/s with a corresponding ion gauge 2 reading of 4.0 μTorr-Xe.

Figure 9 shows the discharge voltage and current waveforms for the thruster operating at 12.5 kW and discharge voltages of 400 V (left) and 800 V (right). As can be seen from Fig. 9, the thruster's discharge becomes more oscillatory at higher discharge voltage operation. Increasing the applied magnetic field slightly reduced the thruster's peak-to-peak (P2P) levels but at the expense of the thruster's performance.

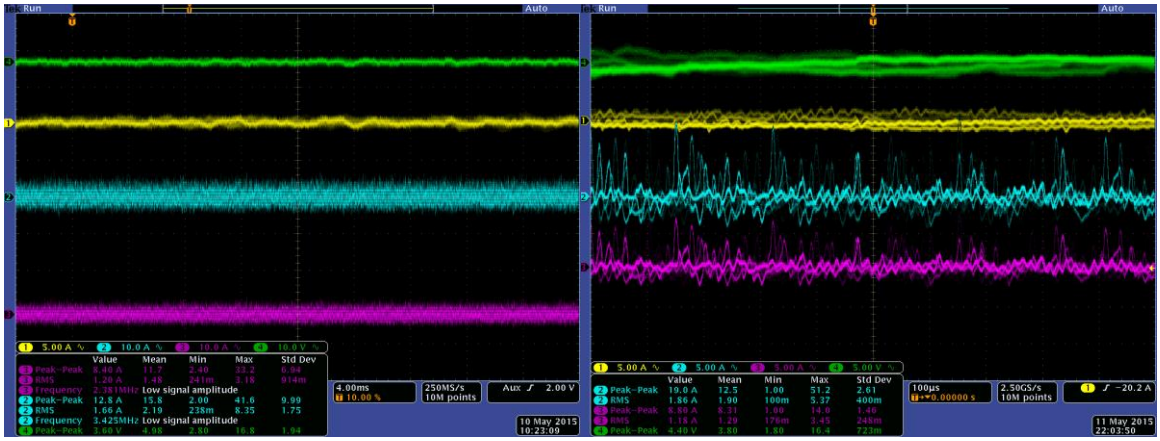

Figure 9. Screen captures of the discharge voltage (green), power supply current (yellow), discharge current from filter capacitor (light blue), and discharge current (purple) waveforms for thruster operation at 12.5 kW at 400 V (left) and 800 V (right) discharge voltages.

Figure 10 presents the P2P/I_d percent. Results in Fig 10 show, in general, that the magnitude increases as the thruster discharge voltage increases, with the highest levels occurring at 800 V thruster operation.

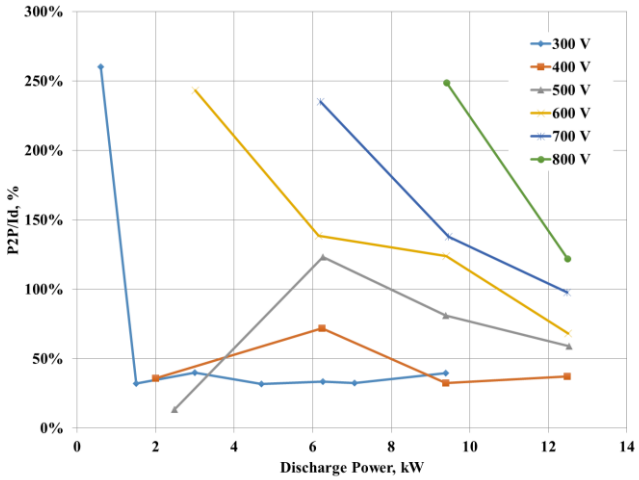

Figure 10. TDU1 P2P/Id % levels at the thruster's various operating conditions.

Figure 11 presents the TDU1 thruster discharge efficiency and specific impulse plots as a function of discharge power. Results in Fig. 11 (left) indicate that for all operating conditions, except at a discharge voltage of 300 V, discharge efficiency increases with discharge power. A peak discharge efficiency of approximately 67% is attained at 12.5 kW and 500 V. For discharge voltages above 500 V, the discharge efficiency drops to approximately 64% at 800 V. Figure 11 (left) also shows that the drop in discharge efficiency with reduced thruster operating power is more pronounced for discharge voltage operation of 700 and 800 V when compared to the other operating discharge voltage magnitudes. Results in Fig. 11 (right) indicate that the discharge specific impulse increases linearly with discharge power. The peak discharge specific impulse of 3,130 s is attained at a discharge voltage of 800 V and 12.5 kW.

Figure 12 present the TDU1 thruster total thrust efficiency and specific impulse. Results is Fig 12 show that the total thrust efficiency and specific impulse increased with increasing thruster power (except for 300 V thruster operation where they remain constant above approximately 4.7 kW). Results in Fig 12 (left) indicate that a peak thrust efficiency of 63% is attained at 12.5 kW. TDU1 operation at 12.5 kW for discharge voltages above 500 V results in reduced total thrust efficiency; a total thrust efficiency of approximately 60% is attained at 800 V. Results in Fig 12 (right) indicate that TDU1's total specific impulse increases linearly with increased discharge power for a given discharge voltage. Results in Fig. 12 show that a peak total specific impulse of 2,960 s is attained at 12.5 kW and 800 V.

The reported thrust efficiencies of the TDU1 thruster are very similar in magnitude to the measured performance of the H6MS and 300MS thrusters.[14,15] Additionally, the peak thrust efficiency that is achieved by a magnetically shielded thruster is typically a few percentage points lower than an unshielded thruster. For the 300MS thruster it was

found that higher beam divergence and lower mass utilization where attained for the 300MS when compared to the unshielded thruster.[27] Analysis of the plasma diagnostics traces from this test are being performed and the phenomenological efficiency model will help elucidate the trends in the processes that govern the overall thrust efficiency.

Finally, The TDU1 thruster performance characterization test results will be used to generate high thrust-to-power, high specific impulse, and high efficiency throttle tables to be used by mission analysts.

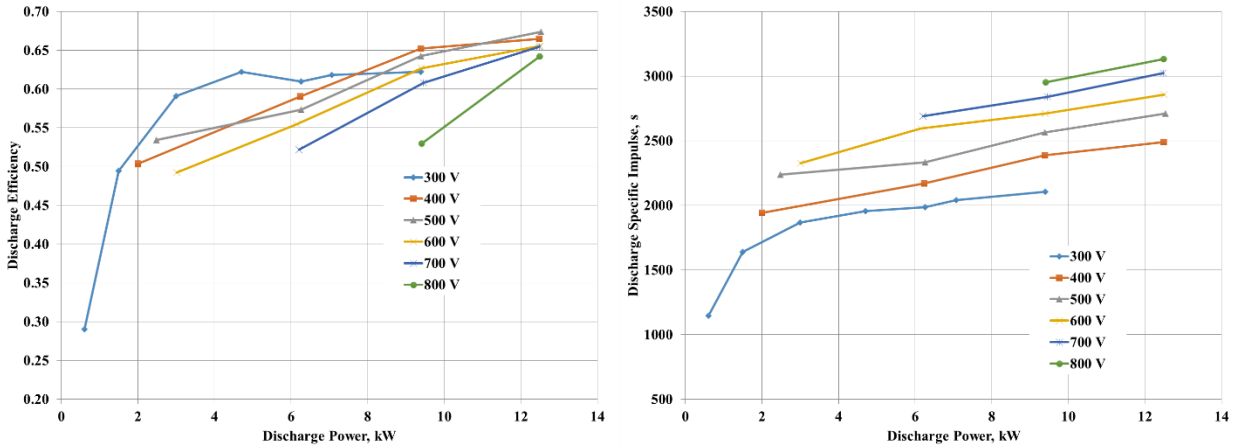

Figure 11. TDU1 discharge efficiency (left) and discharge specific impulse (right) levels for thruster operation at discharge voltages of 300, 400, 500, 600, 700, and 800 V.

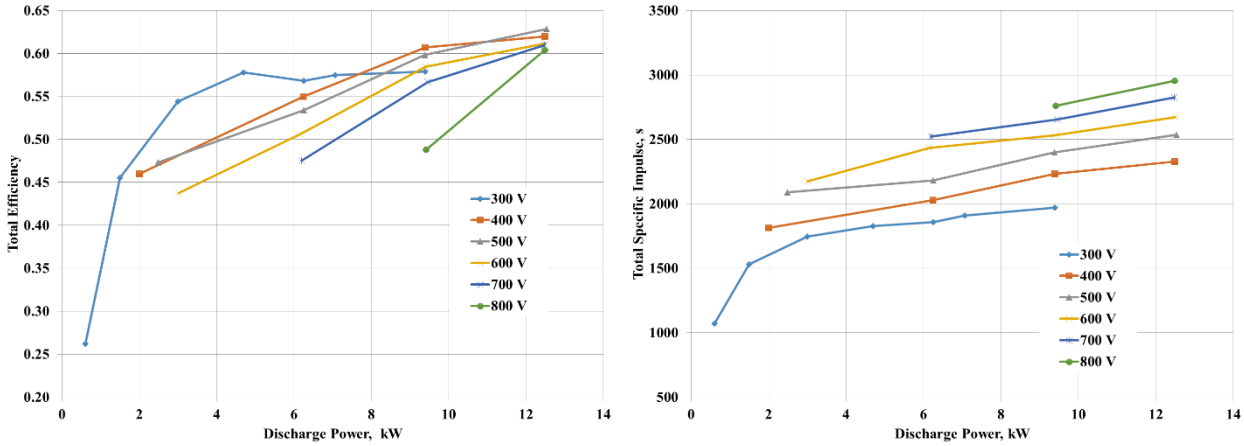

Figure 12. TDU1 total thrust efficiency (left) and specific impulse (right) levels for thruster operation at discharge voltages of 300, 400, 500, 600, 700, and 800 V.

VI. TDU1 Facility Background Pressure Characterization Test Results and Discussion

The facility background pressure characterization test was performed to evaluate the effect of background pressure on the operational characteristics and the performance of the TDU1 thruster. The background pressure of VF5 was elevated by injection of additional xenon via an auxiliary propellant feedline and a 1,000 sccm MFC located at mid-length of the vacuum chamber and pointed downstream of the thruster. The TDU1 thruster was operated at constant discharge power as the facility background pressure was increased. To maintain a constant

Table 5. TDU1 operating conditions during the facility background pressure characterization test.

Discharge Power kW	Discharge Voltage V
4.7, 9.4	300
12.5	400, 500, 600, 700
9.4, 12.5	800

thruster discharge power, the discharge current was kept constant by adjusting the anode mass flow rate as the pressure was increased. In addition, the thruster's magnetic field (electromagnet settings) were optimized during thruster operation at the lowest pressure and were not changed as the thruster was operated at higher background pressure conditions. Table 5 lists the TDU1 thruster operating conditions where testing was performed.

During this test segment the facility background pressure was increased by 1 μTorr until > 10 μTorr pressure was attained. Subsequently, the background pressure was increased by 5 μTorr. Testing was also performed at 1.5× (150% of nominal), 2×, 3×, 4×, and 5× nominal operating pressure and test conditions. Additionally, during this test segment the plasma probe suite and the HS camera were used to collect data. These results are being analyzed and will be presented at the upcoming conference.

Preliminary results were reduced for anode flow rate, thrust, discharge efficiency, P2P/Id %, and cathode-to-ground voltage variations of TDU1 as a function of facility background pressure. Figure 13 presents the anode flow rate variation and the linear fit equations are listed in Table 6. The results show a negatively sloped trend for all the test conditions. This indicates that in order to maintain a constant discharge current, the anode mass flow rate had to decrease with increased facility background pressure, as would be expected. The anode flow rate variation ranged from -0.0149 to -0.0338 mg/s/μTorr (except for operation at 9.4 kW and 800 V due to the very high discharge current oscillations levels resulting in marginally stable thruster operation). For example, at 400 V and 12.5 kW, increasing the background pressure from 6.50 to 25.10 μTorr (about 4× lowest nominal pressure value) required the anode flow rate reduction from 27.55 to 26.66 mg/s, respectively. Hence, a 4× increase in the background pressure only required about 2% decrease in the anode flow rate. For operation at 800 V and 12.5 kW, increasing the background pressure from 3.93 to 14.90 and 19.80 μTorr (about 4× and 5× lowest nominal pressure value) required the anode flow rate reduction from 17.10 to 16.75 and 16.56 mg/s, respectively. Hence, a 4× and 5× increase in the background pressure only required about 2% and 3% decrease in the anode flow rate, respectively. The reductions in the thruster anode flow rate were necessary to compensate for the ingested flow.

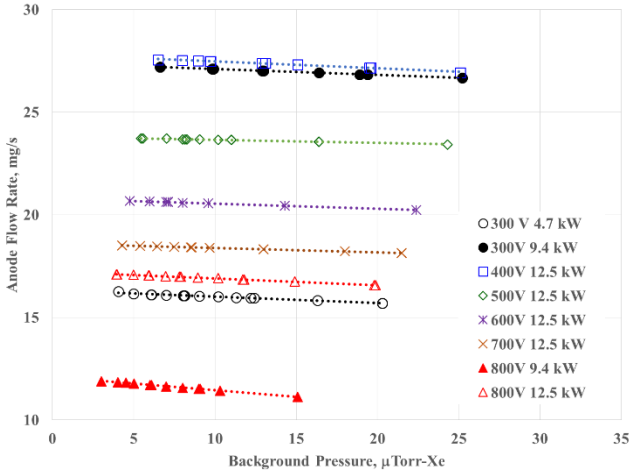

Table 6. TDU1 Anode flow rate linear fit equations from Fig. 13.

Operating Condition	Anode Flow Rate Linear Fit Equation P is pressure in μTorr
300 V 4.7 kW	-0.0315·P+16.326
300 V 9.4 kW	-0.0285·P+27.383
400 V 12.5 kW	-0.0333·P+27.808
500 V 12.5 kW	-0.0149·P+23.805
600 V 12.5 kW	-0.0257·P+20.804
700 V 12.5 kW	-0.0213·P+18.598
800 V 9.4 kW	-0.0641·P+12.094
800 V 12.5 kW	-0.0338·P+17.244

Figure 13. TDU1 anode flow variation as a function of background pressure for various thruster operating conditions.

Figure 14 presents the thrust variation of TDU1 as a function of facility background pressure. A linear fit was applied to the experimental data and resulted in a negatively sloped line for all the test conditions, the linear fit equations are listed in Table 7. The results show that as the background pressure was increased, the anode mass flow rate also decreased (Fig 13 and Table 6) and the thrust dropped very slightly. The equations indicate that the thrust varied by -0.04 to -0.76 mN/μTorr except for the 9.4 kW and 800 V operating condition. For example, at 400 V and 12.5 kW, increasing the background pressure from 6.5 to 25.1 μTorr (about 4× lowest nominal pressure value) resulted in the thrust dropping from 680 to 678 mN, respectively. Hence, a 4× increase in the background pressure resulted in approximately 0.3% decrease in thrust which is less than the accuracy of the thrust measurement. For operation at 800 V and 12.5 kW, increasing the background pressure from 3.93 to 19.8 μTorr (~5× lowest nominal pressure value) resulted in the thrust dropping from 530 to 519 mN. Hence, a 5× increase in the background pressure resulted in about 2% reduction in thrust. These slight drops in thrust are due to corresponding drops in the thruster's anode flow rate that were necessary to maintain TDU1 thruster operation at constant discharge power.

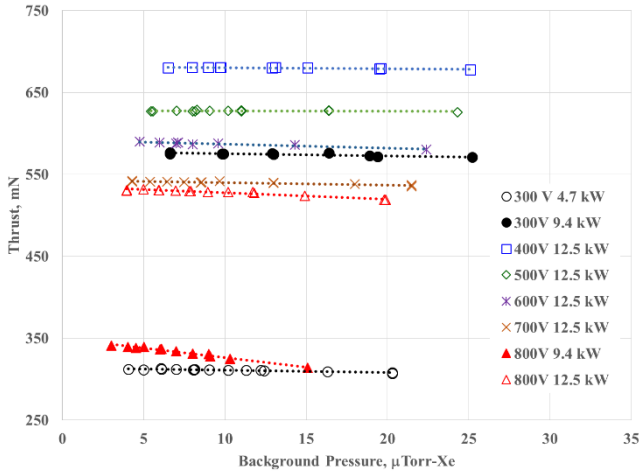

Table 7. TDU1 thrust linear fit equations from Fig 14

Operating Condition	Anode Flow Rate Linear Fit Equation P is pressure in µTorr
300 V 4.7 kW	-0.313·P+314.2
300 V 9.4 kW	-0.268·P+578.1
400 V 12.5 kW	-0.114·P+681.5
500 V 12.5 kW	-0.039·P+627.9
600 V 12.5 kW	-0.497·P+592.0
700 V 12.5 kW	-0.305·P+543.2
800 V 9.4 kW	-2.317·P+349.5
800 V 12.5 kW	-0.761·P+535.2

Figure 14. TDU1 thrust variation as a function of background pressure for various thruster operating conditions.

Figure 15 presents the variation of TDU1 anode efficiency as a function of facility background pressure. The values of anode flow rate and thrust from Figs 13 and 14 were used to compute the anode efficiency variation with pressure. The linear fit equations are presented in Table 8. The results in Fig. 15 and Table 8 show that mixed linear trends were observed. Results in Table 8 show that anode efficiency slightly increases with increased background pressure for 9.4 kW/300 V and 12.5 kW/400, 500, and 700 V; whereas, for thruster operation, at 4.7 kW/300 V, 9.4 kW/800 V, and 12.5 kW/600 and 800 V the anode efficiency decreased as the facility background pressure was increased. Finally, it is important to note that the change in the anode efficiency for all the operating conditions (except for 9.4 kW/800 V) were within the accuracy of the anode efficiency calculation.

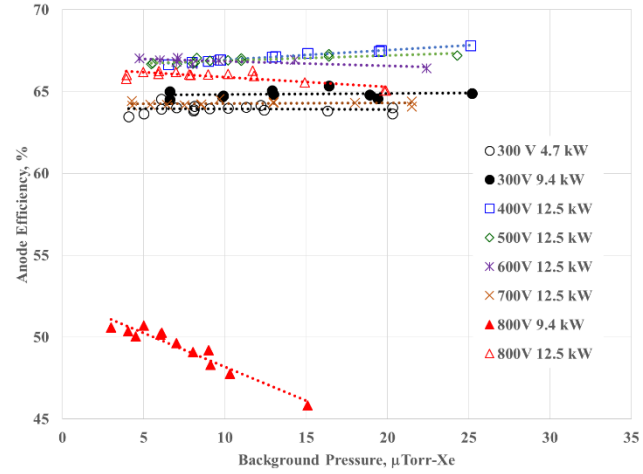

Table 8. TDU1 anode efficiency linear fit equations from Fig 15

Operating Condition	Anode Flow Rate Linear Fit Equation P is pressure in µTorr
300 V 4.7 kW	-0.0023·P +63.95
300 V 9.4 kW	0.0066·P +64.75
400 V 12.5 kW	0.0601·P +66.33
500 V 12.5 kW	0.0320·P +66.56
600 V 12.5 kW	-0.027·P+67.13
700 V 12.5 kW	0.0021·P+64.25
800 V 9.4 kW	-0.413·P+52.33
800 V 12.5 kW	-0.064·P+66.58

Figure 15. TDU1 anode efficiency variation as a function of background pressure for various thruster operating conditions.

Figure 16 presents the P2P/I_d percent variation as a function of background pressure. The findings in Fig.16 indicate that, in general, the facility background pressure did not greatly change the discharge current waveforms oscillation levels. Additionally, the results indicate that the P2P/I_d percent increases as the thruster's discharge voltage is increased (similar trend to Fig. 10). Also, Fig. 16 indicates that at 9.4 kW/800 V operation the thruster was characterized by very high magnitude discharge current oscillations and was becoming unstable. As such trends obtained during TDU1 operation at the condition will not be used to discern operational trends.

Figure 17 presents the cathode-to-ground ($V_{c\text{-}g}$) variation as a function of facility background pressure. The results indicate that $V_{c\text{-}g}$ becomes more negative with increased facility background pressure.

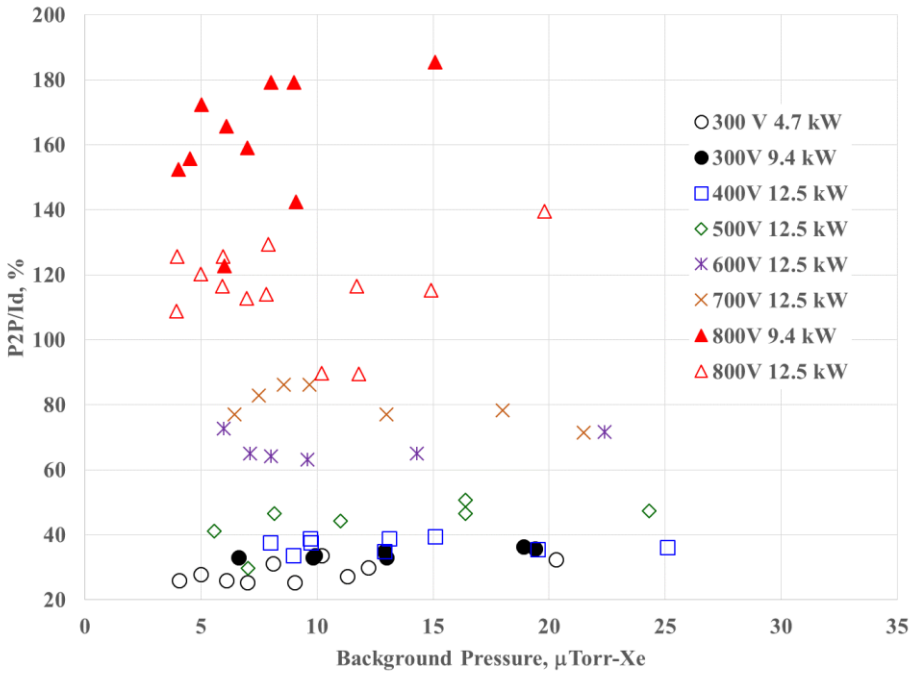

Figure 16. TDU1 P2P/I_d percent variation as a function of background pressure for various thruster operating conditions.

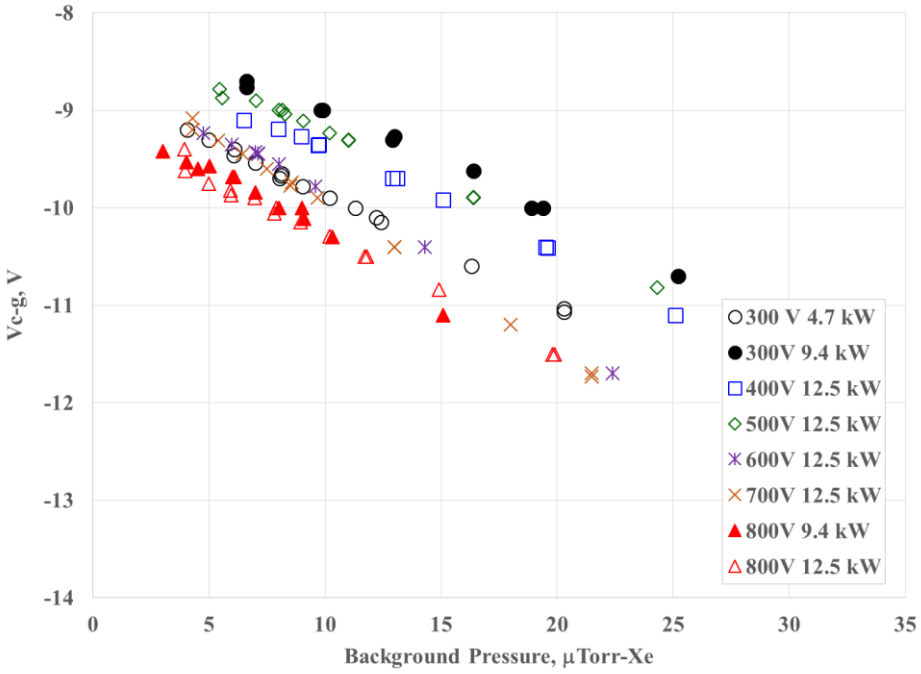

Figure 17. TDU1 $V_{c\text{-}g}$ variation as a function of background pressure for various thruster operating conditions.

Estimates of the ingested flow are made using $\dot{m}_\iota = A_i P \sqrt{\frac{m_{Xe}}{2\pi k_b T_n}}$. The calculations indicate that flow ingestion (at the higher background pressure) does account for the reduction in the anode flow that was necessary to maintain constant discharge current. This is similar to what has been observed by others.[28,29,30,31]

The facility background pressure study found that the TDU1 thruster design was, for the most part, insensitive to changes in the facility background pressure. This is consistent with finding from tests performed on the H6MS and the 300MS thrusters.[15,31] The TDU1 MSCT test indicated that magnetic shielding was effectively maintained at all facility pressures tested.[23] Measured electron temperatures indicated a slight increase at all locations with increasing facility pressure. Previous investigations have observed that the acceleration zone and plasma recede further into the channel towards the anode with elevated facility pressure for unshielded thrusters.[30,32] In particular, this shift was observed to cause increased electron temperatures along the channel walls of the HiVHAc Hall thruster.[32] It is possible that a similar shift in the plasma is occurring towards the anode, resulting in slightly elevated temperatures at higher pressure. However, the magnetically shielded configuration as well as HERMeS's centrally mounted cathode likely make the properties at the channel wall are more insensitive to facility pressure.

Finally, using the linear fit equations presented in Tables 6-8, the TDU1 thruster vacuum performance can be estimated. In general, at a given power level and at "zero" pressure, the TDU1 thruster will require increased anode flow rate and will generate more thrust when compared to its operation in VF5. However, the thruster's anode efficiency will almost remain unchanged from its value during tests at NASA GRC.

VII. Conclusion

NASA's STMD SEP/TDM project is funding the development of a 12.5-kW magnetically-shielded Hall thruster system to support future NASA missions The successful test campaign of the HERMeS TDU1 thruster has demonstrated a viable 12.5-kW class magnetically shielded high specific impulse Hall thruster that has the performance and projected lifetime capability necessary for a suite of NASA TDM missions including the ARM mission.

To date, one HERMeS thruster, TDU1, has been fabricated and extensively tested. A second thruster, TDU2, is under fabrication and will be ready for functional, hot-fire, and environmental tests in September of 2015.

After completing the TDU1 thruster fabrication and performing functional tests, the thruster underwent an extensive test campaign to characterize its plume plasma properties, thermal operation, magnetic shielding, performance, and its operation under elevated facility background pressure levels. The thruster performance was evaluated, its magnetic shielding confirmed, its thermal operation characterized and thermal margins substantiated, and its operational sensitivity to facility background pressure assessed at NASA GRC VF5.

Tests of the thruster confirmed that TDU's magnetic field topology was magnetically shielded, this was confirmed by measurement of the plasma potential and electron temperature along the discharge chamber walls. Inner and outer discharge chamber plasma wall probe measurements found that anode potential and low electron temperatures were attained along the discharge chamber inner and outer wall for all the test conditions. Thermal characterization of the thruster indicated that the thruster can operate at 12.5 kW at a discharge voltage of 800 V and peak radial magnetic field strength and still maintain peak thruster component temperatures below prescribed maximum allowable temperatures.

Performance characterization of the thruster confirmed TDU1's wide throttling ramge capability and found that the thruster can achieve a peak thruster efficiency of 63% at 12.5 kW and can attain a specific impulse of ~3,000 s at 12.5 kW at a discharge voltage of 800 V. Facility background pressure tests revealed that the TDU1 thruster design with a centrally mounted hollow cathode was mostly insensitive to background pressure changes. Tests at full power revealed that increasing VF5 background pressure by 5× resulted in only a 2% drop in thrust for constant power thruster operation.

Detailed data analysis from the various TDU1 test segments is still ongoing and results will be presented at upcoming conferences in 2015 and 2016. The remaining data analysis tasks include:

- analysis of all the thermal characterization test thermocouple data and comparison with the thermal model;
- analysis of the FP, ExB, RPA, and LP data analysis and inclusion of results in a phenomenological model to help elucidate thruster measured efficiency;
- analysis of the high speed camera video to provide insights into TDU1's operating modes and mode transitions;
- analysis of the discharge current waveforms and generation of power spectral density (PSDs) plots; and
- I-V-B sweeps at different facility background pressure levels to help elucidate thruster stability regime.

Additional tests of the TDU1 thruster are planned for late 2015 and 2016. Upcoming TDU1 tests will include front pole plasma property measurements and an extended duration wear test of at least 2,000 hrs. After completion of the TDU2 thruster fabrication at NASA GRC in September of 2015, it will undergo functional and baseline hot-fire tests

at NASA GRC. It will then be shipped to JPL for environmental tests. Tests at JPL will be performed to evaluate the fidelity of the design against expected thermal and structural loads.

Acknowledgments

The authors would like to thank and acknowledge the Space Technology Mission Directorate (STMD) for funding this work as well as Mike Barrett and David Irimies, SEP-TD Project and Deputy Project managers, respectively. The authors would like to thank and acknowledge the other members of the HERMeS team, including Chris Griffith (lead thruster mechanical designer), Lauren Clayman (IPS Thermal Engineer), Timothy Verhey (IPS Cathode Lead), John Steven Snyder (IPS lead system engineer), Benjamin Jorns (IPS thruster diagnostics engineer), and Dan Goebel (IPS thruster diagnostics, cathode engineer and senior research scientist). The authors would also like to thank and acknowledge Kevin Blake, George Jacynycz, Terry Jansen, Roland Gregg and Drew Fausnaugh for providing facility support and their significant contributions with thruster installation during this test campaign.

References

[1] Dudzinski, L., et al., "Design of Solar Electric Propulsion Transfer Vehicle for a Non-Nuclear Human Mars Exploration Architecture," IEPC Paper 99-181, October 1999.

[2] Oleson, S.R., et al., "Advanced Propulsion for Space Solar Power Satellites," AIAA Paper 99-2872, June 1999.

[3] Oleson, S.R., et al., "Mission Advantages of Constant Power Variable Specific Impulse Electrostatic Thrusters," NASA TM-2000-210477, March 2000.

[4] McGuire, M. L., Hack, K. J., Manzella, D. H., and Herman, D. A., " Concept designs for NASA's Solar Electric Propulsion Technology Demonstration Mission," AIAA-2014-3717, 50th AIAA/ASME/SAE/ASEE Joint Propulsion Conference, Cleveland, OH, July 28-30, 2014.

[5] Manzella, D., and Hack, K., "High-Power Solar Electric Propulsion for Future NASA Missions," AIAA-2014-3718, 50th AIAA/ASME/SAE/ASEE Joint Propulsion Conference, Cleveland, OH, July 28-30, 2014.

[6] Brophy, J.R., et al., "300-kW Solar Electric Propulsion System Configuration for Human Exploration of Near Earth Asteroids," AIAA Paper 2011-5514, August 2011.

[7] Hofer, R. R. and Randolph, T. M., "Mass and Cost Model for Selecting Thruster Size in Electric Propulsion Systems," Journal of Propulsion and Power 29, 1, 166-177 (2013).

[8] Smith, B., Nazario, M. L., and Manzella, D. H., "Advancement of a 30kW Solar Electric Propulsion System Capability for NASA Human and Robotic Exploration Mission," IAC-12-C4.4.2.

[9] Brophy, et. al., "Near-Earth Asteroid Retrieval Mission (ARM) Study," IEPC-2013-082.

[10] Herman, D. A., et al., "The Development of the Ion Propulsion System for the Solar Electric Propulsion Technology Demonstration Mission", *34th International Electric Propulsion Conference*, IEPC-2015-008, Hyogo-Kobe, Japan, July 4-10, 2015.

[11] K.H. De Grys, A. Mathers, B. Welander, V. Khayms, AIAA Paper No. 10-6698, in: Proceedings of the 46th AIAA/ASME/SAE/ASEE Joint Propulsion Conference, Nashville, TN, 2010, pp. 6698.

[12] Mikellides, I.G., Katz, I., Hofer, R. R., *et al.*, "Magnetic shielding of the channel walls in a Hall plasma accelerator," *Physics of Plasmas*, vol. 18, no. 3, pp. 033501, Mar, 2011.

[13] I. G. Mikellides, I. Katz, R. R. Hofer *et al.*, "Magnetic shielding of a laboratory Hall thruster. I. Theory and validation," *Journal of Applied Physics*, vol. 115, no. 4, Jan 28, 2014.

[14] R. R. Hofer, D. M. Goebel, I. G. Mikellides *et al.*, "Magnetic shielding of a laboratory Hall thruster. II. Experiments," *Journal of Applied Physics*, vol. 115, no. 4, Jan 28, 2014.

[15] Kamhawi, H., et al., "Performance and Thermal Characterization of the NASA-300MS 20 kW Hall Effect Thruster," Proceedings of the 33rd International Electric Propulsion Conference, IEPC-2013-444, Washington, D.C., October 6-10, 2013.

[16] Shastry, R., Huang, W., Haag, T. W., and Kamhawi, H., "Langmuir Probe Measurements within the Discharge Channel of the 20-kW NASA-300M and NASA-300MS Hall Thrusters", *33rd International Electric Propulsion Conference*, IEPC-2013-122, Washington, D.C., October 6-10, 2013.

[17] Hofer, R. R., Kamhawi, H., Herman, D. A., Polk, J. E., and Mikellides, I. G., "Development Approach and Status of the 12.5 kW HERMeS Hall Thruster for the Solar Electric Propulsion Technology Demonstration Mission", *34th International Electric Propulsion Conference*, IEPC-2015-186, Hyogo-Kobe, Japan, July 4-10, 2015.

[18] Huang, W., Yim, J., and Kamhawi, H, "Design and Empirical Assessment of the HERMeS Hall Thruster Propellant Manifold", *62nd JANNAF Propulsion Meeting*, JANNAF-2015-XXXX, Nashville, TN, June 1-5, 2015.

[19] Shastry, R., Herman, D. A., Soulas, G. C., and Patterson, M. J., "End-of-test Performance and Wear Characterization of NASA's Evolutionary Xenon Thruster (NEXT) Long-Duration Test", 50th AIAA/ASME/SAE/ASEE Joint Propulsion Conference, Cleveland, OH, July 28-30, 2014.

[20] Goebel, D. M. and Chu, E., "High-Current Lanthanum Hexaboride Hollow Cathode for High-Power Hall Thrusters," Journal of Propulsion and Power 30, 1, 35-40 (2014).

[21] Kamhawi, H., et al., "Overview of the Development of the Solar Electric Propulsion Technology Demonstration Mission 12.5-kW Hall Thruster", *50th AIAA/ASME/SAE/ASEE Joint Propulsion Conference*, AIAA-2014-3898, Cleveland, OH, July 28-30, 2014.

[22] Yim, J. T., and Burt, J. M., "Characterization of Vacuum Facility Background Gas Through Simulation and Considerations for Electric Propulsion Ground Testing", 51st AIAA/ASME/SAE/ASEE Joint Propulsion Conference, AIAA-2015-xxxx.

[23] Shastry, R., Huang, W., and Kamhawi, H.,, "Near-Surface Plasma Characterization of the 12.5-kW NASA TDU1 Hall Thruster", 51st AIAA/ASME/SAE/ASEE Joint Propulsion Conference, AIAA-2015-xxxx.

[24] Huang, H., Kamhawi, H., Myers., J. L., Yim, J., and Neff, G., "Non-Contact Thermal Characterization of NASA's 12.5-kW Hall Thruster", 51st AIAA/ASME/SAE/ASEE Joint Propulsion Conference, AIAA-2015-xxxx.

[25] Williams, G., and Kamhawi, H., "Optical Characterization of Component Wear and Near-Field Plasma of the HERMeS Thruster", *62nd JANNAF Propulsion Meeting*, JANNAF-2015-XXXX, Nashville, TN, June 1-5, 2015.

[26] Mikellides, I. G., et al., "Hall2de Simulations of a 12.5-kW Magnetically Shielded Hall Thruster for the NASA Solar Electric Propulsion Technology Demonstration Mission", *34th International Electric Propulsion Conference*, IEPC-2015-254, Hyogo-Kobe, Japan, July 4-10, 2015.

[27] Huang, H., Shastry, R., Soulas, G., and Kamhawi, H., "Farfield Plume Measurement and Analysis on the NASA-300M and NASA-300MS*", 33rd International Electric Propulsion Conference*, IEPC-2013-057, Washington, D.C., October 6-10, 2013.

[28] Walker, M. L. R., "Effects of Facility Backpressure on the Performance and Plume of a Hall Thruster," Ph.D. Dissertation, Aerospace Engineering, University of Michigan, Ann Arbor, MI, 2005.

[29] Azziz, Y., and Martinez-Sanchez, M., "Experimental and Theoretical Characterization of a Hall Thruster Plume," Ph.D. Dissertation, Department of Aeronautics and Astronautics, Massachusetts Institute of Technology, Cambridge, MA, 2007.

[30] Kamhawi, H., Huang, W., Haag, T., and Spektor, R., "Investigation of the Effects of Facility Background Pressure on the Performance and Voltage-Current Characteristics of the High Voltage Hall Accelerator", *50th AIAA/ASME/SAE/ASEE Joint Propulsion Conference*, AIAA-2014-3707, Cleveland, OH, July 28-30, 2014.

[31] Hofer, R. R., and Anderson, J. R., "Finite Pressure Effects in a Magnetically Shielded Hall Thrusters", *50th AIAA/ASME/SAE/ASEE Joint Propulsion Conference*, AIAA-2014-3709, Cleveland, OH, July 28-30, 2014.

[32] Shastry, R., Kamhawi, H., Huang, W., and Haag, T. W., "Experimental Investigation of the Near-Wall Region in the NASA HiVHAc EDU2 Hall Thruster", *34th International Electric Propulsion Conference*, IEPC-2015-246, Hyogo-Kobe, Japan, July 4-10, 2015